Transmitter-receiver-transmitter-configured ground-penetrating radars over randomly heterogeneous ground models

Levent Gürel and Uğur Oğuz

Department of Electrical and Electronics Engineering, Bilkent University, Bilkent, Ankara, Turkey

Received 8 September 2001; revised 8 January 2002; accepted 26 April 2002; published 16 November 2002.

[1] Ground-penetrating radar (GPR) problems are simulated using the finite-difference time-domain (FDTD) method. The GPR model is configured with arbitrarily polarized three antennas, two of which are transmitting antennas fed 180° out of phase. The receiver is placed in the middle of two transmitters, where it receives no direct coupling from the transmitting antennas. The ground is modeled as a dielectric, lossy, and heterogeneous medium. The performances of the transmitter-receiver-transmitter-configured GPRs above the heterogeneous ground models are investigated. The computational domain is terminated by perfectly matched layer (PML) absorbing boundaries. The PML is adapted to match both air and ground regions of the computation space. *INDEX TERMS:* 0933 Exploration Geophysics: Remote sensing; 3210 Mathematical Geophysics: Modeling; 0659 Electromagnetics: Random media and rough surfaces; 6969 Radio Science: Remote sensing; *KEYWORDS:* ground-penetrating radar, finite-difference time-domain method, perfectly matched layer

Citation: Gürel, L., and U. Oğuz, Transmitter-receiver-transmitter-configured ground-penetrating radars over randomly heterogeneous ground models, *Radio Sci.*, *37*(6), 1094, doi:10.1029/2001RS002528, 2002.

1. Introduction

[2] The ground-penetrating radar (GPR) [*Daniels*, 1996] is used to explore underground patterns and detect buried targets by transmitting electromagnetic waves into the ground and observing the reflected waves. Therefore, the basic elements of a GPR unit are the transmitting and the receiving antennas, whose designs depend on the specifications of the particular application. The design of the antennas may vary with the type of the soil, and also the characteristics, shape, and possible depth of the target. However, apart from the special features of a particular application, the same problems are encountered in almost all GPR scenarios: the waves scattered from the target are not the only signals observed at the receiver since the receiver collects waves coupled directly from the transmitter, reflected from the ground-air interface, and scattered from other scatterers embedded in the ground. Therefore, the signals scattered from the actual target should be isolated from the other signals in order to be able to extract the correct information.

0048-6604/02/2001RS002528$11.00

[3] Among various electromagnetic modeling techniques that have been applied to simulate GPR problems [*Bourgeois and Smith*, 1996; *Moghaddam et al.*, 1991a], the finite-difference time-domain (FDTD) [*Yee*, 1966] is known for its adaptability to multilayered problems involving an arbitrary number of inhomogeneities [*Moghaddam et al.*, 1991b; *Demarest et al.*, 1995], and thus the method, whose popularity rapidly grew in the last two decades, has been frequently used for GPR simulations [*Bourgeois and Smith*, 1998; *Teixeria et al.*, 1998]. This paper also employs the FDTD method to model and simulate the GPR problems. In addition, perfectly matched layer (PML) [*Berenger*, 1994; *Fang and Wu*, 1996] absorbing boundary conditions (ABCs) are used to terminate the computational domain. Similar to the FDTD method, the PML ABC is easily adapted to the layered media and it can terminate both the ground and the air regions simultaneously, without any extra effort [*Verdu et al.*, 1995; *Gürel and Oğuz*, 2000].

[4] In this paper, the simulation results of a specific type of a GPR configuration are presented in order to assess its performance over lossy and heterogeneous grounds. The referred GPR configuration consists of two transmitters and a receiver placed in the middle of the other two [*Gürel and Oğuz*, 2000; *Luneau and Delisle*, 1996]. When the two transmitting antennas are

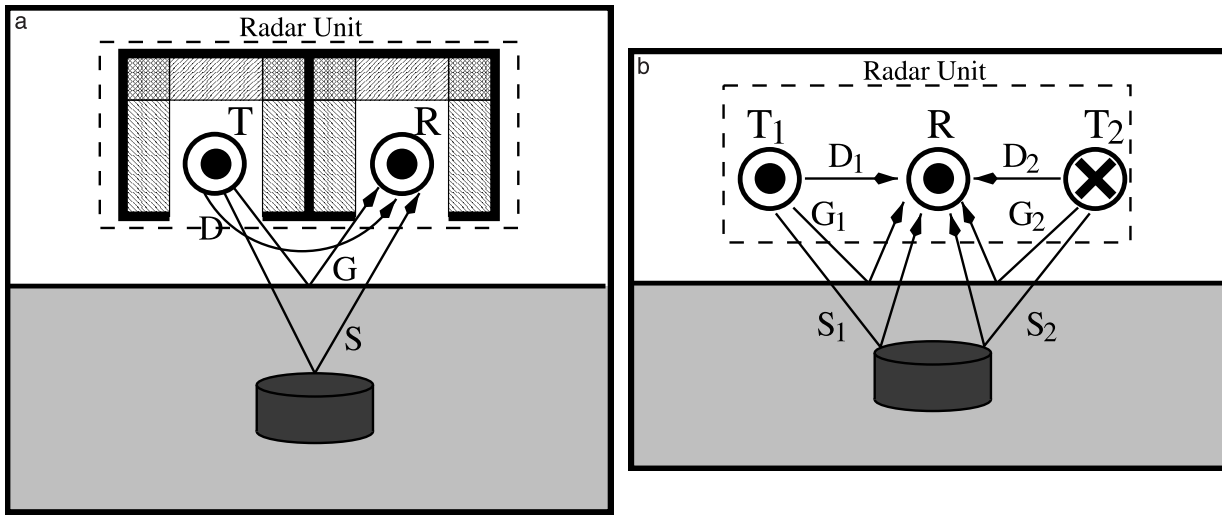

Figure 1. (a) Transmitter-receiver (TR) and (b) transmitter-receiver-transmitter (TRT) configurations of the radar unit and the definition of the direct (D, D_1, and D_2), reflected (G, G_1, and G_2), and scattered (S, S_1, and S_2) signals.

fed 180° out of phase, a symmetry plane exists exactly in the middle of these two antennas, on which the waves emitted by the transmitters cancel each other. Placing the receiver on this plane, as displayed in Figure 1b, yields the elimination of the most of the undesired signals at the receiver. Figure 1a and 1b display the transmitter-receiver (TR) and transmitter-receiver-transmitter (TRT) configurations of the GPR, respectively. The TR configuration results in the direct coupling (D) of the transmitter signals to the receiver, which are much larger than the scattered signals (S). In order to decrease the amplitude of D by isolating the transmitter and the receiver, a conducting shield, supported by absorbers mounted on the inner walls [*Gürel and Oğuz*, 1999; *Oğuz and Gürel*, 2001b], can be used, as demonstrated in Figure 1a. Such a shield model does not completely eliminate the direct coupling, but decreases the amplitude of the D signal down to tolerable levels [*Oğuz and Gürel*, 2001b]. The simulation results obtained with this GPR model over heterogeneous and lossy ground models are reported by *Gürel and Oğuz* [2001]. The simulation results obtained with the TRT configuration over homogeneous and lossless ground models are also reported [*Gürel and Oğuz*, 2000, 2002; *Oğuz and Gürel*, 2001a]. This paper investigates the performance of the TRT configuration of GPR over lossy and heterogeneous grounds.

2. GPR Models With TRT Configurations

[5] Figure 2 displays the four GPR models with TRT configurations, referred to as GPR1, GPR2, GPR3, and GPR4. These four models are introduced by *Gürel and Oğuz* [2000], and the typical differences of their outputs are also demonstrated in the same paper. The differences between the outputs of GPR1, GPR2, GPR3, and GPR4 are results of the different alignment and polarizations of the transmitting and receiving antennas in the TRT configuration. In GPR1 and GPR2, all the antennas are horizontally polarized, whereas GPR3 and GPR4 employ vertically polarized antennas. For GPR1 and GPR3, the alignment of the antennas are perpendicular to the path of the radar unit. However, in GPR2 and GPR4, all the antennas are aligned in the direction of radar-unit movement. The path traversed by the radar unit is illustrated in Figure 3.

[6] In this work, the transmitting antennas are small dipoles modeled by single cells of constant current densities. These current sources are excited with a smooth transient pulse given by

$$J(t) = \left[4(4\pi f_0 t)^3 - (4\pi f_0 t)^4\right] e^{-4\pi f_0 t}, \qquad (1)$$

where f_0 is the center frequency of the pulse and Δ, Δt are the spatial and temporal sampling periods, respectively. Due to the constant current density character of the transmitters, the above expression should be divided by a factor of Δ^3 to obtain the correct amount of total induced current [*Buechler et al.*, 1995].

[7] The receiver is modeled as a small probe that samples and stores the x, y, or z component of the electric-field function, depending on the selection of the GPR model. Denoting the arbitrary polarization with v, the samples of the electric-field function, $E_v(x, y, z, t)$, computed by the FDTD scheme at every Δt seconds, are

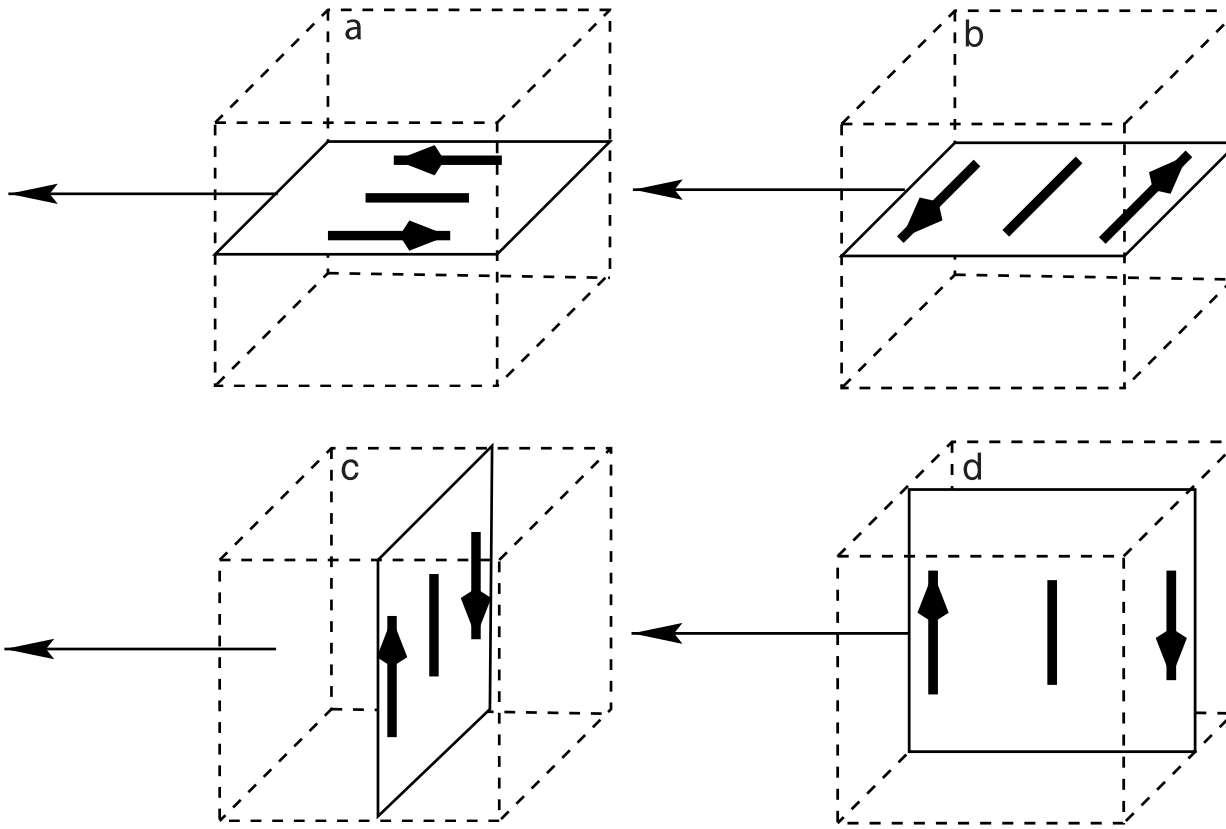

Figure 2. The four TRT-configured GPR models: (a) GPR1, (b) GPR2, (c) GPR3, and (d) GPR4.

stored in a set of data. When the radar unit collects data at a stationary point (x_0, y_0, z_0), this is called an A-scan, and the resulting data is denoted as

$$E_v^n = E_v(x_0, y_0, z_0, n\Delta t). \tag{2}$$

A B-scan is obtained by performing repeated A-scan measurements at discrete points on a linear path. If the radar unit moves in the x direction, the B-scan data is denoted as

$$E_v^{i,n} = E_v(i\Delta x, y_0, z_0, n\Delta t). \tag{3}$$

[8] In the work of *Gürel and Oğuz* [2000] the separation between the transmitting and receiving antennas was set as 5 mm for all four GPR models. However, the work of *Gürel and Oğuz* [2002] and *Oğuz and Gürel* [2001a] demonstrated that this separation value was far from optimum for the simulation scenario involving a 2.5-cm-radius disk buried 5 cm under the ground. In the work of *Gürel and Oğuz* [2002] and *Oğuz and Gürel* [2001a], it was demonstrated that a separation of 6 cm between the transmitters and the receiver yielded the maximum observed scattered-field energy. All the simulation results presented in this paper are obtained with 6 cm separation between the transmitting and receiving antennas. The radar unit travels at an elevation of 5 cm above the ground-air interface. The center frequency of the transmitted pulse in (1) is 500 MHz. The spatial and temporal

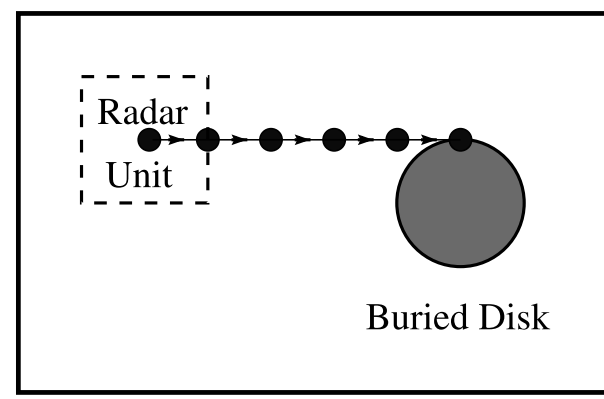

Figure 3. Bird's eye view of the GPR path employed in the simulation results presented in Figures 4, 6, 8. The GPR unit travels along a linear path until the receiver reaches the projection of the center of the conducting disk.

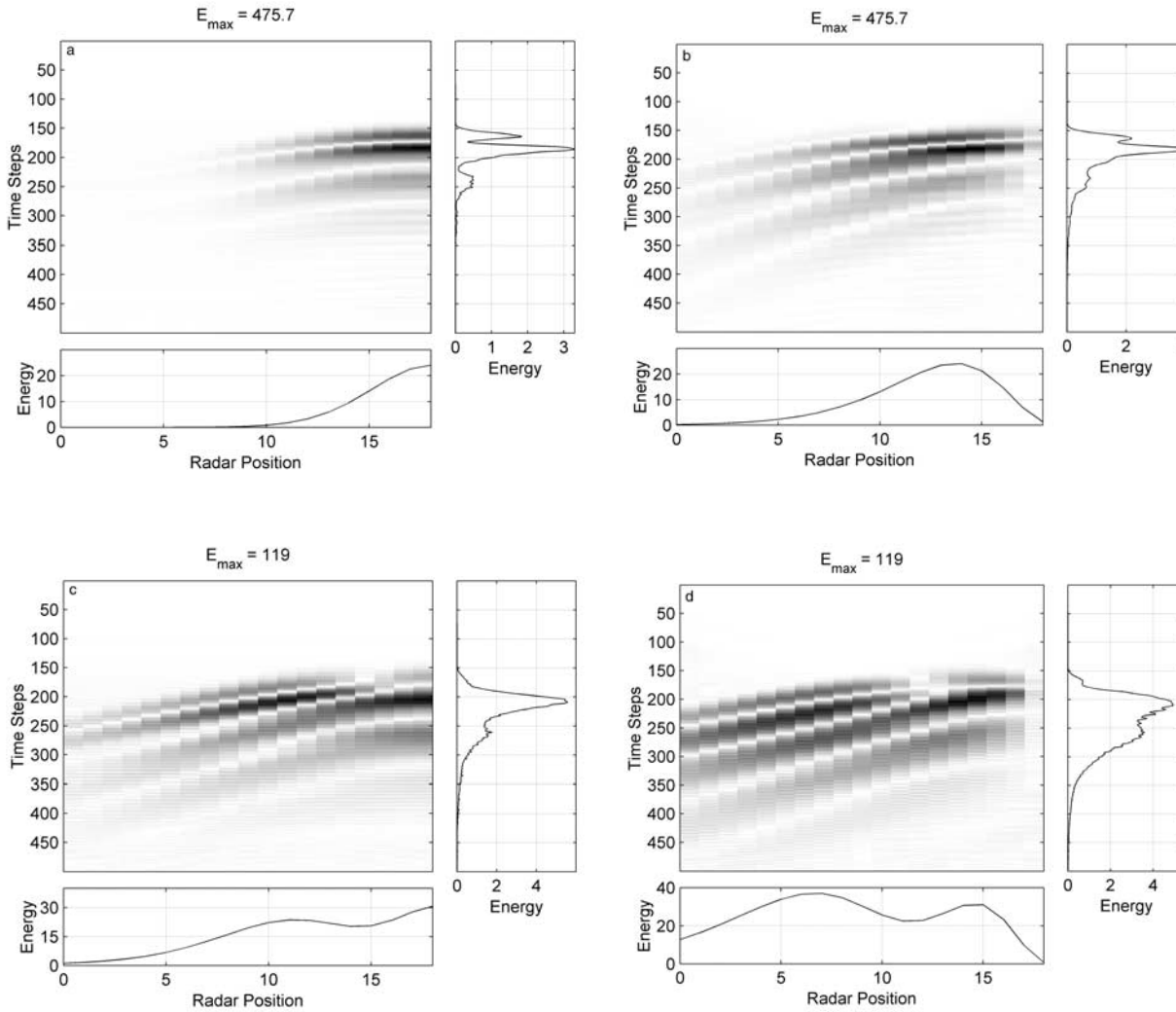

Figure 4. B-scan results of a buried dielectric disk obtained with (a) GPR1, (b) GPR2, (c) GPR3, and (d) GPR4. The ground is a homogeneous, dielectric, and conducting half space.

sampling periods, Δ and Δt, are 5 mm and 9 ps, respectively. These parameters are kept fixed in all simulation results presented in this paper.

[9] Figure 4 presents the simulation results of a dielectric disk, which is buried 5 cm under the ground. The curvature of the disk is modeled using the contour-path algorithms [*Jurgens et al.*, 1992]. The radius and height of the disk are set as 2.5 cm and 4 cm, respectively. The disk has a permittivity of $3\epsilon_0$ and zero conductivity, while the ground is modeled with $8\epsilon_0$ permittivity and 0.01 S/m conductivity. The B-scan signals in Figures 4a, 4b, 4c, and 4d are recorded by GPR1, GPR2, GPR3, and GPR4, respectively, all of which travel 5 cm above the ground and along a path whose projection is tangent to the buried disk, as shown in Figure 3. In these B-scan images, the vertical axes represent the time steps, which can also be interpreted as the depth into the ground, and the horizontal axes represent the radar position. Due to the printed-space considerations, Figures 4, 6, and 8 present only "half plots," i.e., the radar unit approaches the buried object and stops at a position, where the center of the disk is located, as depicted in Figure 3. Nevertheless, the omission of the other halves of the plots does not affect the results deduced from these B-scan simulations.

[10] A careful investigation of Figures 4a–4d reveals that GPR1 and GPR3 produce similar results, and the outputs of GPR2 and GPR4 resemble each other. Therefore, the alignment of the antennas plays a major role in

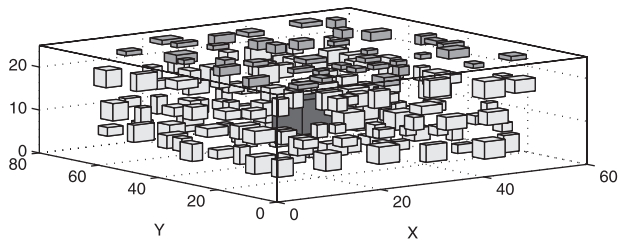

Figure 5. The heterogeneous ground model, which contains surface holes (darker boxes), underground scatterers, and the actual target.

the B-scan measurements. GPR1 and GPR3 produce visible responses only when the radar unit is close to the target, while GPR2 and GPR4 are more sensitive to distant targets. Due to the symmetry in the problem, there exist minima in the B-scan measurements performed by GPR2 and GPR4, when these two models are exactly above the target. However, GPR1 and GPR3 collect the maximum scattered fields at the same position.

[11] In addition to the B-scan images, each of Figures 4a–4d displays two additional energy plots. These two plots, which are located below and to the right of the B-scan image, display the cumulative energy received at each particular time step and at each radar position of the B-scan measurement, respectively. Denoting the recorded B-scan data as $E_v^{i,n}$, which is defined in (3), the energy plot below the B-scan image is computed by

$$\text{Energy}^i = \sum_n \left| \frac{E_v^{i,n}}{\max_{i,n}\left(E_v^{i,n}\right)} \right|^2, \tag{4}$$

where $\max_{i,n}(E_v^{i,n})$, the maximum of the observed B-scan electric-field data, is the normalization factor. Similarly, the energy plot placed to the right of the B-scan image is given by

$$\text{Energy}^n = \sum_i \left| \frac{E_v^{i,n}}{\max_{i,n}\left(E_v^{i,n}\right)} \right|^2, \tag{5}$$

where $\max_{i,n}(E_v^{i,n})$ is again the normalization factor. Therefore, the energy plot below the B-scan image is related to the position of the target, and the plot on the right indicates the depth of the target. These two plots below and to the right of the B-scan images are referred to as constant-position and constant-depth energy plots, respectively.

3. Heterogeneous Ground Models

[12] Above a homogeneous ground model, the scattering signal is the only signal collected by the receiver since, in addition to the directly coupled signals, the signals reflected from the ground-air interface also cancel each other. However, this is not a realistic situation since heterogeneity is an invariable feature of real-life soils. In the work of *Gürel and Oğuz* [2001], such soils were simulated in the context of TR-configured GPR models employing shields and absorbers. The TRT configuration can be preferred to the TR configuration for its performance over homogeneous soils. However, the effects of ground inhomogeneities and especially surface roughness should be studied in order to assess the overall performance of the TRT configuration. For this reason, a simulation setup employing a heterogeneous ground model and a TRT-configured GPR is designed. The ground model has a volume of $80 \times 80 \times 25$ Yee cells and is designed so that the density of the heterogeneities is the same as that of "the densely heterogeneous ground model" of *Gürel and Oğuz* [2001]. The main features of the heterogeneous ground model used in this work, which is illustrated in Figure 5, are as follows:

1. The background permittivity and conductivity are $8\ \epsilon_0$ and 0.01 S/m, respectively.

2. In the upper level of the ground, which also contains the ground-air interface, there are 40 holes, with ϵ_0 permittivity and zero conductivity. These holes create a surface roughness at the ground-air interface.

3. There are 40 highly conducting small objects in the middle level of the ground. This level of the ground models the humid part of real-life soils, where many conducting objects, such as plant roots or wet spots, are present. The sizes, locations, permittivities, and conductivities of these objects are randomly selected. The permittivity and the conductivity values of these objects lie between ϵ_0–$16\epsilon_0$ and 0.1–0.2 S/m, respectively.

4. In the third level of the ground, in addition to the actual target, 80 dielectric and conducting objects are placed. Although the same range of permittivity values (ϵ_0–$16\epsilon_0$) is used for the scatterers in this level, they are designed to be less conductive than the scatterers in the middle level by randomly choosing the conductivity values between 0.03–0.04 S/m.

5. The holes on the surface have a minimum width of 1 cm, a maximum width of 2 cm, and a maximum depth of 1 cm. The x, y, and z dimensions of the scatterers in the second and third layers of the ground are randomly selected between 0.5 cm and 1.5 cm.

[13] Using this heterogeneous ground model and a buried dielectric disk, four simulations are performed with the four TRT-configured GPR models, and the results are displayed in Figure 6. The modeled dielectric disk is identical to the one employed in the previous section and it is buried to the same depth, i.e., 5 cm under the ground-air interface. The B-scan results obtained with GPR1, GPR2, GPR3, and GPR4 are shown in Figures 6a, 6b, 6c, and 6d, respectively. Comparison of Figures 6a–6d to 4a–4d reveals the effects of the surface and ground inhomogeneities. Figures 6a and 6b demon-

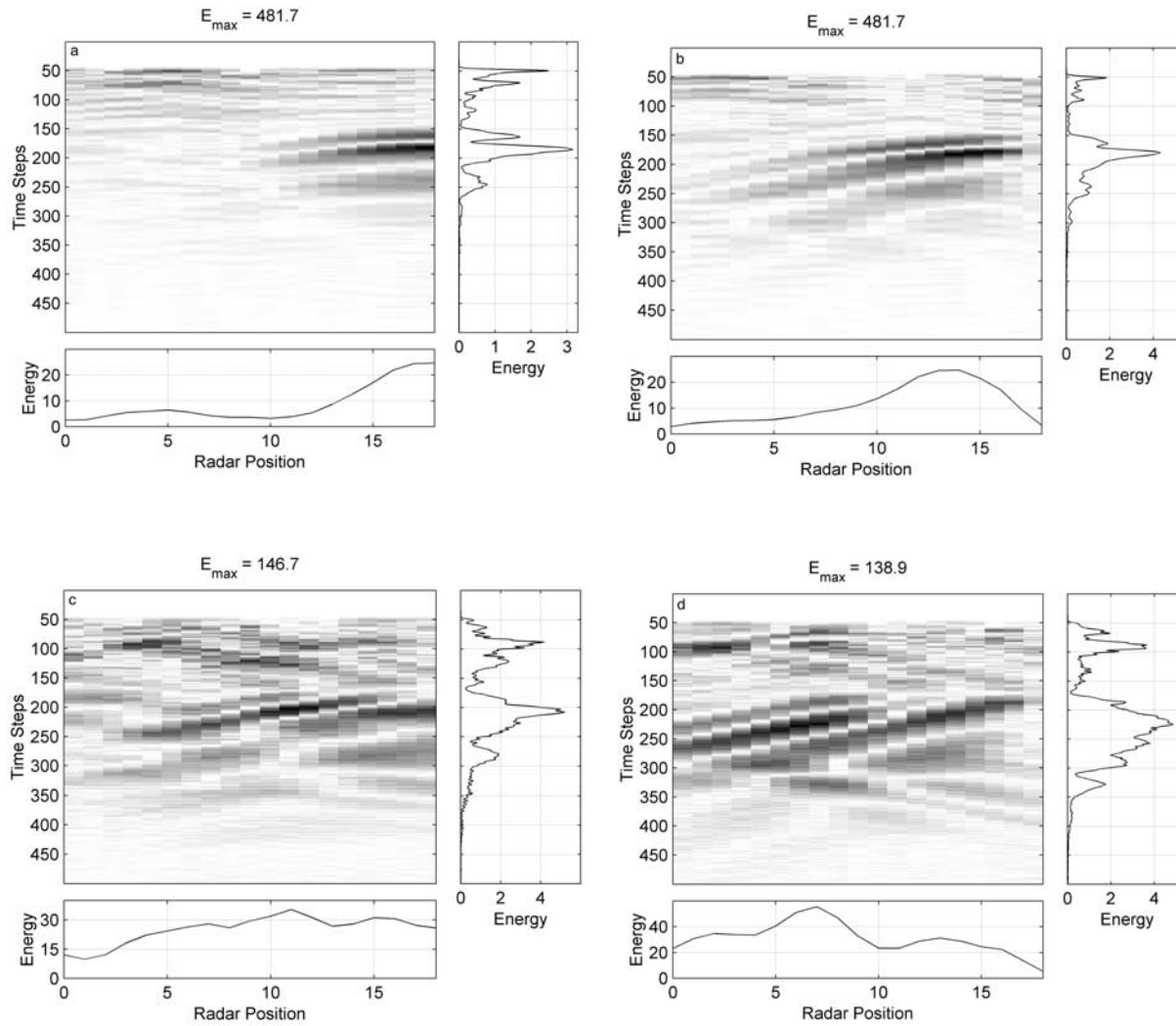

Figure 6. B-scan results of a buried dielectric disk obtained with (a) GPR1, (b) GPR2, (c) GPR3, and (d) GPR4. The ground is heterogeneous and contains randomly placed surface holes and small scatterers of arbitrary permittivity and conductivity.

strate that the waves scattered from the dielectric disk are dominant in the overall B-scan images of GPR1 and GPR2, and the nonuniformity on the ground surface does not prevent the detection of the target. The constant-depth and constant-position energy plots in Figures 6a and 6b also demonstrate the satisfactory performances of GPR1 and GPR2 above heterogeneous ground models. However, the performances of GPR3 and GPR4 are adversely influenced from the ground heterogeneities and surface roughness, as demonstrated in Figures 6c and 6d. Moreover, the energy peaks in the constant-position and constant-depth plots in Figures 6c and 6d do not indicate the correct location of the dielectric disk.

[14] Constant-depth energy plots of Figures 6a and 6b demonstrate that GPR1 and GPR2 produce ''energy spikes'' exactly at the surface level. These spikes can easily be eliminated by even the simplest detection algorithms, thus revealing the depth of the actual target. On the other hand, GPR3 and GPR4 produce energy peaks at later times, or equivalently, corresponding to the inhomogeneities underground. These energy peaks are considerably more difficult to distinguish from the scattered energy of the actual target. Therefore, considering the surface holes and the underground inhomogeneities altogether, we conclude that GPR1 and GPR2 have better performances than GPR3 and GPR4.

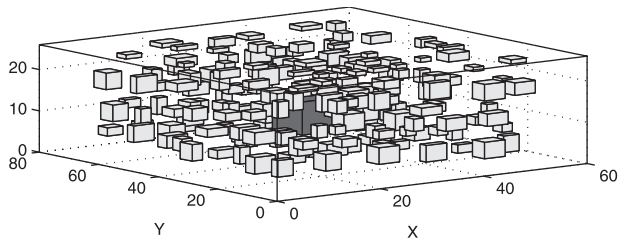

Figure 7. The altered heterogeneous ground model, which contains underground scatterers and the actual target, but no surface holes.

[15] In order to further demonstrate the sensitivities of different TRT configurations to the surface roughness, another set of simulations are performed, where the ground is still heterogeneous, but the ground-air interface is converted to a smooth surface. For this purpose, the aforementioned heterogeneous ground model is altered by moving all small scatterers and the target one cell deeper into the ground. Therefore, the dielectric disk is buried 5.5 cm deep in the ground, and the small holes in the surface are transformed into cavities, or rather air bubbles, in the ground. This ground model is illustrated in Figure 7. Figures 8a–8d present the simulation results

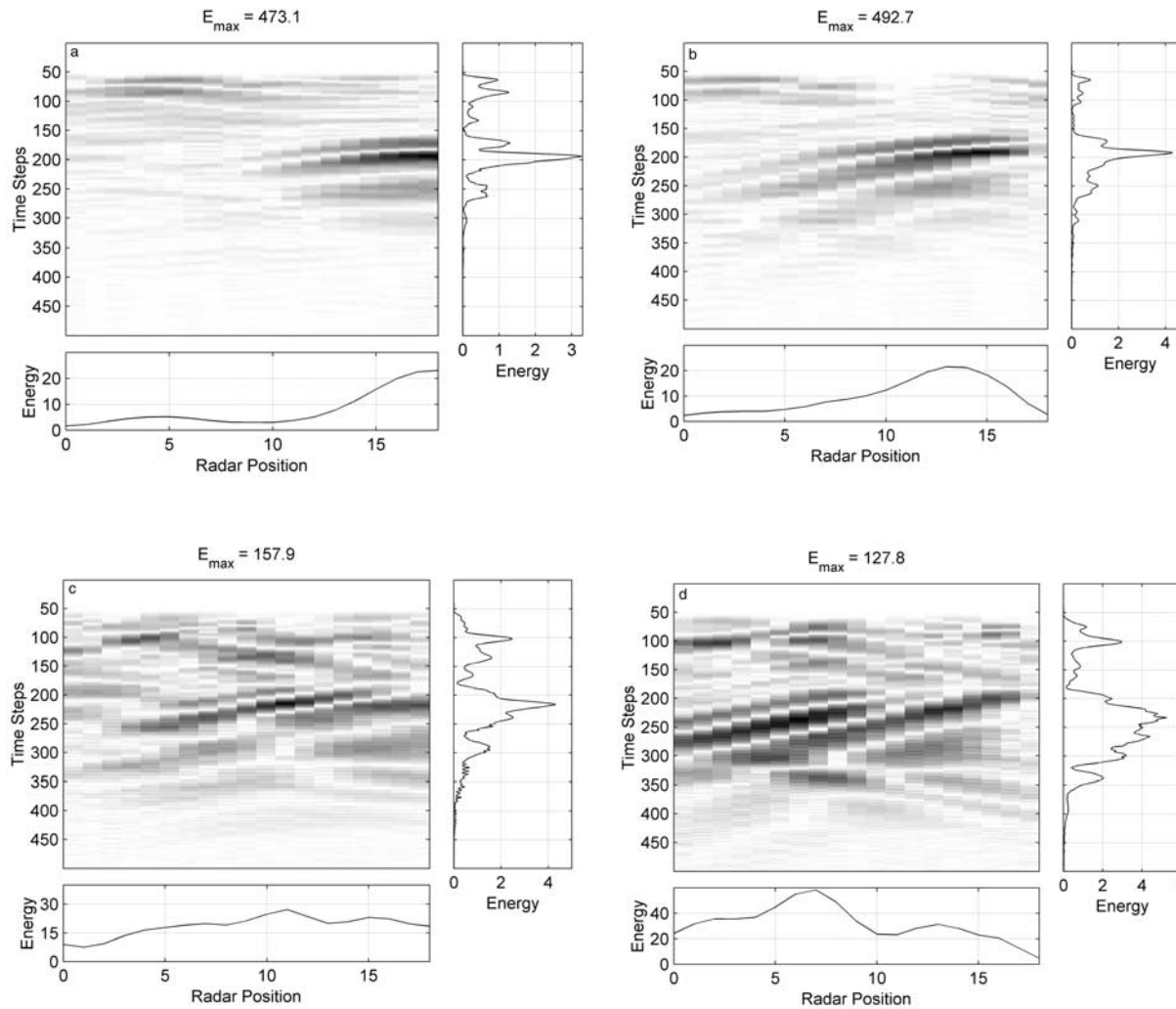

Figure 8. B-scan results of a buried dielectric disk obtained with (a) GPR1, (b) GPR2, (c) GPR3, and (d) GPR4. The ground surface is smooth but the ground itself contains randomly placed small scatterers of arbitrary permittivity and conductivity. The holes in Figure 6 are transformed into cavities 5 mm under the surface.

obtained with this altered heterogeneous ground model. Comparison of Figures 8a–8d to Figures 6a–6d reveal the sensitivities of the four TRT-configured GPR models to the surface scatterers. Figures 8a and 8b demonstrate that the ''energy spikes'' observed at the surface level of the constant-depth energy plots of Figures 6a and 6b are no longer present. Therefore, the detection of the buried target by GPR1 and GPR2 is clearly facilitated by the removal of surface scatterers. However, Figures 8c and 8d do not depict such effective decreases in the energies of the waves scattered from the surface or close-to-surface objects. Therefore, comparison of Figures 8c and 8d to Figures 6c and 6d reveals that GPR3 and GPR4 are not especially sensitive to the surface roughness, but quite sensitive to the underground inhomogeneities.

[16] In the work of *Gürel and Oğuz* [2001], a similar test on surface scatterers was performed with the TR-configured GPR model. That test produced conclusions similar to those obtained for GPR1 and GPR2 in this work. Noting that the TR-configured GPR model of *Gürel and Oğuz* [2001] includes horizontally polarized dipoles, similar to GPR1 and GPR2, it is clear that the transmitting and receiving antenna polarizations have major influence on the detection performance of the GPR.

4. Concluding Remarks

[17] GPR simulations employing lossy and heterogeneous ground models are performed. An arbitrary ground model is used, in which the inhomogeneities in the ground are allowed to have random location, size, permittivity, and conductivity. The surface inhomogeneities also have arbitrary location and size, but their permittivity and conductivity values are set equal to that of air. Apart from the small scatterers embedded in the ground, the ground is modeled as a homogeneous and conducting medium, and the air is modeled as free space. The buried target is modeled as a dielectric disk, which is implemented using the contour-path algorithms for a better approximation.

[18] The GPR unit is modeled by two transmitters and a receiver placed exactly in the middle of them. In this configuration, feeding the two transmitters with opposite phases yields the cancellation of the waves coupled directly from the transmitters to the receiver. However, there exist other noise signals in the total received signal, which are due to the waves reflected from the ground-air interface and the waves scattered from the ground inhomogeneities. A smooth ground-air interface causes the cancellation of waves reflected from the ground-air interface, due to the symmetry. Similarly, if the target is the only inhomogeneity in the ground, then the total received signal is purely composed of the desired signals scattered from the target. However, such ideal circumstances are never encountered in real-life GPR problems, and the receiver collects many other signals in addition to the desired scattered signal. The performance of the GPR unit over such inhomogeneous grounds is of major importance.

[19] In this work, four different TRT-configured GPR models are simulated over lossy and heterogeneous ground models. These models have different polarizations and alignments of the transmitting and receiving antennas. Simulation results reveal that GPR models employing horizontally polarized antennas (GPR1 and GPR2) are more sensitive to the surface roughness, which is simulated by random nonuniformities (holes) on the surface of the ground. However, GPR1 and GPR2 also produce better signal-to-noise ratios in the heterogeneous-ground simulations compared to GPR3 and GPR4, which employ vertically polarized antennas.

[20] **Acknowledgments**. This work was supported by Bilkent University under research fund EE-01-01.

References

Berenger, J. P., A perfectly matched layer for the absorption of electromagnetic waves, *J. Comput. Phys.*, *114*(1), 185–200, 1994.

Bourgeois, J. M., and G. S. Smith, A fully three-dimensional simulation of a ground-penetrating radar: FDTD theory compared with experiment, *IEEE Trans. Geosci. Remote Sens.*, *34*(1), 36–44, 1996.

Bourgeois, J. M., and G. S. Smith, A complete electromagnetic simulation of the separated-aperture sensor for detecting buried land mines, *IEEE Trans. Antennas Propag.*, *46*(10), 1419–1426, 1998.

Buechler, D. N., D. H. Roper, C. H. Durney, and D. A. Christensen, Modeling sources in the FDTD formulation and their use in quantifying source and boundary condition errors, *IEEE Trans. Microwave Theory Tech.*, *43*(4), 810–814, 1995.

Daniels, D. J., *Surface-Penetrating Radar*, IEE, London, England, 1996.

Demarest, K., R. Plumb, and Z. Huang, FDTD modeling of scatterers in stratified media, *IEEE Trans. Antennas Propag.*, *43*(10), 1164–1168, 1995.

Fang, J., and Z. Wu, Generalized perfectly matched layer for the absorption of propagating and evanescent waves in lossless and lossy media, *IEEE Trans. Microwave Theory Tech.*, *44*(12), 2216–2222, 1996.

Gürel, L., and U. Oğuz, Employing PML absorbers in the design and simulation of ground penetrating radars, paper presented at Institute of Electrical and Electronics Engineers AP-S International Symposium and USNC/Union Radio Scientific Internationale National Radio Science Meeting, Orlando, Fla., July 1999.

Gürel, L., and U. Oğuz, Three-dimensional FDTD modeling of a ground-penetrating radar, *IEEE Trans. Geosci. Remote Sens.*, *38*(4), 1513–1521, 2000.

Gürel, L., and U. Oğuz, Simulations of ground-penetrating radars over lossy and heterogeneous grounds, *IEEE Trans. Geosci. Remote Sens.*, *39*(6), 1190–1197, 2001.

Gürel, L., and U. Oğuz, Optimization of the transmitter-receiver separation in the ground-penetrating radar, *IEEE Trans. Antennas Propag.*, in press, 2002.

Jurgens, T. G., A. Taflove, K. Umashankar, and T. G. Moore, Finite-difference time-domain modeling of curved surfaces, *IEEE Trans. Antennas Propag.*, *40*(4), 357–366, 1992.

Luneau, P., and G. Y. Delisle, Underground target probing using FDTD, paper presented at Institute of Electrical and Electronics Engineers AP-S International Symposium and Union Radio Scientifique Internationale Radio Science Meeting, Baltimore, Md., July 1996.

Moghaddam, M., E. J. Yannakakis, W. C. Chew, and C. Randall, Modeling of the subsurface interface radar, *J. Electromagn. Waves Appl.*, *5*(1), 17–39, 1991a.

Moghaddam, M., W. C. Chew, B. Anderson, E. J. Yannakakis, and Q. H. Liu, Computation of transient electromagnetic waves in inhomogeneous media, *Radio Sci.*, *26*(1), 265–273, 1991b.

Oğuz, U., and L. Gürel, The effects of the antenna separation and polarization on the simulation results of transmitter-receiver-transmitter-configured ground-penetrating radars, Bilkent Univ., Bilkent, Ankara, Turkey, 28 March 2001a. (Available at http://www.cem.bilkent.edu.tr/gpr/)

Oğuz, U., and L. Gürel, Modeling of ground-penetrating-radar antennas with shields and simulated absorbers, *IEEE Trans. Antennas Propag.*, *49*(11), 1560–1567, 2001b.

Teixeria, F. L., W. C. Chew, M. Straka, and M. L. Oristaglio, Finite-difference time-domain simulation of ground-penetrating radar on dispersive, inhomogeneous, and conductive soils, *IEEE Trans. Geosci. Remote Sens.*, *36*(6), 1928–1937, 1998.

Verdu, J. B., R. Gillard, K. Moustadir, and J. Citerne, An extension of the PML technique to the FDTD analysis of multilayer planar circuits and antennas, *Microwave Opt. Technol. Lett.*, *10*(6), 323–327, 1995.

Yee, K. S., Numerical solution of initial boundary value problems involving Maxwell's equations in isotropic media, *IEEE Trans. Antennas Propag.*, *14*(4), 302–307, 1966.

L. Gürel and U. Oğuz, Department of Electrical and Electronics Engineering, Bilkent University, TR-06533 Bilkent, Ankara, Turkey. (lgurel@ee.bilkent.edu.tr)